SINTERING AND ROBOCASTING OF β-TRICALCIUM PHOSPHATE SCAFFOLDS FOR ORTHOPAEDIC APPLICATIONS

Pedro Miranda*, Eduardo Saiz, Karol Gryn, Antoni P. Tomsia

Materials Sciences Division, Lawrence Berkeley National Laboratory.
1 Cyclotron Rd. Berkeley, CA 94720

* Guest Scientist at MSD, Lawrence Berkeley National Laboratory
from Departamento de Electrónica e Ingeniería Electromecánica. Universidad de Extremadura.
Avda de Elvas s/n. 06071 Badajoz, Spain

Accepted for Publication in Acta Biomaterialia

November, 2005

ABSTRACT

β-tricalcium phosphate (β-TCP) scaffolds with designed, three-dimensional (3-D) geometry and mesoscale porosity have been fabricated by direct-write assembly (robocasting) techniques. Concentrated β-TCP inks with suitable viscoelastic properties were developed to enable the fabrication of the complex 3-D structures. A comprehensive study of the sintering behavior of TCP as a function of the calcium content in the starting powder was also carried out, and the optimal heat treatment for fabricating scaffolds with dense β-TCP rods has been determined. Such analysis provides clues to controlling the microstructure of the fabricated structures and, therefore, enabling the fabrication by robocasting of TCP scaffolds with tailored performance for bone tissue engineering applications.

Key Words: robocasting, sintering, tricalcium phosphate, scaffolds, bone tissue engineering

I. INTRODUCTION

The most desirable way to repair damaged bone is to regrow natural, undamaged bone in its place. Unfortunately, if large volumes of tissue are removed, the body is simply not able to regrow an entirely new piece of bone (e.g., a new hip joint). In these cases the need for an artificial substitute is unavoidable. The ideal bone substitute would be a material that will form a secure bond with the tissues by allowing and encouraging new cells to invade. One way to achieve this is to use a material that is osteoconductive and porous, so that new tissue, and ultimately new bone, can be induced to grow into the pores to prevent loosening and movement of the implant. Such porosity must be interconnected to allow the ingrowth of cells, vascularization, and diffusion of nutrients. An ideal three-dimensional (3-D) porous scaffold would provide the necessary support for cells to proliferate and would slowly degrade and resorb as the tissue structures grow *in vitro* and/or *in vivo* [1].

The optimal scaffold design and fabrication techniques must be able to create porous structures adequate to attaining the desired mechanical function and mass transport properties (permeability and diffusion properties). In conventional porous scaffold fabrication methods—such as solvent casting in combination with particulate leaching, fiber meshing, gas foaming, melt molding, freeze drying, phase separation, and supercritical-fluid technology, among others [2,3]—it is difficult to precisely control pore size, geometry and spatial distribution, to create internal channels within the scaffold for vascularization, and to produce scaffolds within arbitrary and complex 3-D anatomical shapes.

Solid freeform fabrication (SFF) techniques [3-9] provide a means to overcome these obstacles, producing scaffolds with customized shape and predefined, reproducible internal morphology without the need for subsequent machining. SFF technologies—three-

dimensional printing, stereolithography, fused deposition modeling, robocasting, phase-change jet printing, etc.—involve building 3-D objects from a computer-aided design (CAD) model using layered manufacturing strategies. These techniques have the additional advantage that data obtained from computerized tomography (CT) or magnetic resonance imaging (MRI) medical scans can be used to create the CAD model and consequently match the scaffold's external shape to the damaged tissue site. Moreover, most of these techniques can be used to fabricate structures with different materials combinations, creating microstructural and chemical gradients or patterns with tailored functionality.

Robocasting—also referred as direct-write assembly—is unique among these processes because it allows one to build ceramic scaffolds using water-based inks with minimal organic content (< 1 wt%) and without the need for a sacrificial support material or mold [10-12]. This technique consists of the robotic deposition of highly concentrated colloidal suspensions (inks) capable of fully supporting their own weight during assembly, thanks to their carefully tailored composition and viscoelastic properties. In this work, we report the development of concentrated β-TCP inks suitable for direct-write assembly of scaffolds consisting of a 3-D network of β-TCP rods (characteristic diameters of ~200 μm and up) with tailored geometry and mesoscale porosity.

Several scaffold materials have been investigated for tissue engineering bone and cartilage, but special attention has been devoted to calcium phosphate compounds because of their ability to directly bond to hard tissue [13-14]. Tricalcium phosphate (TCP, $Ca_3(PO_4)_2$) bioceramics exhibit a higher biodegradability (higher resorption rate) than other appealing candidates such as hydroxyapatite (HA, $Ca_{10}(PO_4)_6(OH)_2$), the main inorganic component of bone [15]. Higher solubility can be beneficial in some applications.

Research with calcium phosphate coatings suggests that the presence of Ca and PO_4 ions released through dissolution near an implant may be more conducive to bone formation than the absence of such ions (i.e., an insoluble surface) [16]. Local supersaturation of the constituent ions of the bone mineral phase, arising from an enhanced solution of calcium phosphate, may cause enhanced bone growth [17]. It was found that more soluble α-TCP coatings evoked more bone remodeling activity than the more stable HA coatings during the first weeks of implantation [17].

Among the three allotropic forms of TCP, β-TCP is preferred as a bioceramic because of its chemical stability, mechanical strength, and intermediate bioresorption rate [18]. However, the difficulties involved in fully densifying β-TCP powders are well documented [18-20] and are usually attributed to the need to keep sintering temperatures low to avoid transformation to α-TCP. Although improvements in the densification of β-TCP have been sought through the use of additives and wet-chemical routes [20,21], few systematic studies have been devoted to investigating its sintering behavior.

Therefore, a comprehensive sintering study of β-TCP powders was carried out to determine the optimal heat treatment for the printed scaffolds. According to the calcium phosphates phase diagram and because of the inability of TCP to deviate from stochiometry, the calcium-to-phosphorous (Ca/P) ratio was promptly identified as a key variable for sintering behavior. Subsequently, the effect of CaO content in the powders was systematically investigated. As expected, the behavior of calcium-rich (Ca/P>1.5) and calcium-deficient (Ca/P<1.5) samples was found to be significantly different, with the latter leading to pure β-TCP samples with higher density and the former transforming completely to α-TCP at the tested temperatures with no improved densification. This

sintering analysis provides clues to controlling the microscopic porosity within the rods that form the scaffolds, which may prove essential in determining their osteointegration properties.

Finally, the hardness of the printed TCP rods was surveyed by indentation and compared with that of β-TCP bulk samples. These scaffolds may find potential application as implant materials for bone tissue engineering, and the reported results provide significant clues towards the optimization of such direct-write assembled TCP structures.

II. EXPERIMENTAL PROCEDURE

(1) Powder characterization

Commercially available β-TCP (Fluka, Buchs, Switzerland) powders were used to prepare inks for robocasting. The average particle size of the as-received powders was 1.8 ± 0.8 μm, as measured by centrifugal photo-sedimentation (Capa 700, Horiba Instruments Inc., Irvine, CA), and a Ca/P molar ratio of 1.348 was measured by inductively coupled plasma mass spectrometry (ICP-MS), implying that the as-received powder is calcium-deficient (Ca/P<1.5). In order to study the effect of CaO content on the sintering behavior, TCP and $CaCO_3$-99% (JT Baker, Phillipsburg, NJ) powders were mixed in a ball mill for 1 hour using zirconia balls. The mixture was then reacted at 1200ºC for 2 hours in air.

In order to study the effect of the powder morphology on the ink properties, some batches of the as-received TCP powder were calcined in air at 1000ºC and 1200ºC for times up to 6 hours. All calcined powders were sieved through 38 μm mesh to remove hard

agglomerates, and several batches were subsequently refined in an attritor mill (Szegvari Attritor 01-HD, Union Process Inc., Akron, OH) with zirconia balls (3 mm diameter) at 450 rpm for 1 hour.

(2) Sintering study

The sintering of TCP was studied using bulk green samples fabricated by isostatic pressing at 170 MPa. First, a dilatometry study was performed on samples with increasing CaO content in a standard dilatometer (DIL-1600, Orton, Westerville, OH) with alumina push rod and holder at a heating rate of 3ºC/min. The starting powders and sintered samples were characterized by X-ray diffraction (D500, Siemens AG, Munich, Germany) using Cu Kα radiation (wavelength 1.54 Å) to determine whether any phase changes occurred during sintering. Bulk samples and final assembled scaffolds were imaged using scanning electron microscopy (SEM) (S-4300SE/N, Hitachi America Ltd., Tarrytown, NY) to analyze their microstructural evolution. Average grain sizes were determined by using the mean linear intercept method (ASTM Standard E 112-88). In addition, the sintered density, ρ, and open porosity, P_{open}, of the samples was characterized using Archimede's method [22].

(3) Scaffold fabrication

Robocasting inks were prepared by first making a stable suspension with 40-50 vol% of powder in distilled water [12]. The stability of the suspension was achieved by dissolving the appropriate amount of Darvan® C dispersant (R.T. Vanderbilt, Norwalk, CT) in the water and then gradually adding the powder while shaking vigorously after each addition. The mixture, together with a few zirconia grinding balls, was subsequently placed in a paint shaker (Red Devil 5400, Red Devil Equipment Co., Plymouth, MN) for about 1 hour to improve its homogeneity and stability. An appropriate amount (7 mg per ml of

solution) of previously dissolved hydroxypropyl methylcellulose (Methocel F4M, Dow Chemical Company, Midland, MI) was then added to the mixture to increase viscosity. Subsequently, the ink was gellified by adding the proper amount of polyethylenimine (PEI) as flocculant. The viscosity of the final ink was modified to desired consistency by adjusting its pH with HNO_3 or NH_4OH as needed. Each addition to the mixture was followed by shaking for about 1 hour in the paint shaker. The final quality of the ink was assessed in terms of printability—measured as the minimum tip diameter suitable to extrude the ink without clogging—and stability (i.e., shape retention capacity during drying and sintering) of the assembled structures.

The optimum amount of dispersant and flocculant to be used in the robocasting ink was determined by analyzing the sedimentation of suspensions (10 vol%) after 24 hours in test tubes. The suspensions had increasing amounts of dispersant (with no flocculant) or flocculant (at optimal amount of dispersant) and were mixed in a paint shaker for 2 hours using alumina balls.

β-TCP 3-D scaffolds of various geometries were constructed via direct-write assembly of the fabricated inks using a robotic deposition device (3-D Inks, Stillwater, OK). The printing syringe was partially filled with the ink, tapped vigorously under slight vacuum to remove bubbles, and then placed on the 3-axis motion stage controlled independently by a computer-aided direct-write program (Robocad 3.0, 3-D Inks, Stillwater, OK). The pastes were deposited through conical deposition nozzles (smooth-flow tapered tips, EFD Inc., East Providence, RI) of different diameters (from 250 μm up to 1.55 mm) at the volumetric flow rate required to maintain a constant x-y printing speed.

Deposition was made in a non-wetting oil bath to prevent non-uniform drying during assembly. Thus, a 3-D network of β-TCP rods was obtained, as shown in Figure 1.

The resulting samples were dried in air at room temperature for 24 hours and then at 400ºC (1ºC/min heating rate) for 1 hour to evaporate organics, followed by the appropriate sintering treatment at temperatures ranging from 1250ºC to 1550ºC (heating rate 3ºC/min), depending on the starting powders, and sintering times of from 2 to 6 hours.

(4) Mechanical characterization

Microindentation Vickers tests (Micromet 1600, Buehler, Lake Bluff, IL, USA) were performed at 0.49-N loads on polished cross-sections of selected scaffolds to measure the hardnesses of the robocasted TCP lines and compare them to bulk isostatically pressed samples sintered under the same conditions. Evaluation of the intrinsic mechanical properties of the TCP rods composing the structure is essential to provide input parameters for numerical simulations (for example by finite element modeling) that would eventually allow optimization of the scaffolds' mechanical performance through intelligent design of their geometry. Microindentation was selected as mechanical test tool—instead of nanoindentation or macroscopic techniques such as uniaxial testing—because its intermediate probe scale allows analysis of the effect of microscopic defects within the structure (intrinsic porosity, microcracks) without effect from the macroscopic geometry of the scaffold.

Preliminary uniaxial compression tests were performed at 0.01 mm/s crosshead speed in ~2 x 2 x 2.5 mm samples, which were cut from the printed scaffolds using a diamond saw.

III. RESULTS AND ANALYSIS

(1) Selection of the appropriate sintering treatment

The first step in this study was to determine the optimal sintering treatment for the fabrication of the scaffolds. Looking at the CaO-P_2O_5 phase diagram [23] (Fig. 2), it is clear that depending on the amount of calcium oxide, CaO, the appropriate sintering treatment should be radically different. Solid-state sintering of Ca-deficient TCP (Ca/P<1.5) would be limited to temperatures up to ~1288ºC—where liquid phases are expected to form and, therefore, the shape of the scaffolds could be jeopardized—while calcium-rich (Ca/P>1.5) powders could be sintered in solid state up to about 1578ºC.

Preparation of β-TCP powders with exact stoichiometry (Ca/P=1.5) in a consistent manner can be difficult and the densification behaviors expected for Ca-rich and Ca-deficient material are very different. A way to ensure that the materials are reproducible is to systematically work with powders that are in one of the zones of the phase diagram, either Ca-rich or Ca-deficient. In this way small changes in composition will not affect the sintering behavior and properties.

Consequently, four batches of powder with increasing amounts of CaO (0.5, 1, 3, and 6 wt%) were prepared from the as-received powders (Ca/P=1.348) by solid-state reaction with $CaCO_3$ at 1200ºC for 2 hours, to analyze the effect of calcium content in the sintering behavior of TCP by dilatometry (Figure 3). The results show that increasing the amount of CaO in the starting powders diminishes the shrinkage rate. Also evident is the

difference in behavior between Ca-deficient (solid lines) and Ca-rich (dashed lines) samples. Ca-deficient samples exhibit almost no shrinkage up to around the eutectic temperature (1288ºC), where a liquid phase is expected to form and shrinkage rate increases dramatically. The as-received powder sample is an exception to this, with its densification starting at lower temperature thanks to the high specific surface area of the uncalcined powders, which permits higher reactivity in solid state. In addition, the as-received sample's initial green density is also lower because irregular particles are more difficult to pack. On the other hand, Ca-rich samples show slow but steady shrinkage from about 1200ºC up to 1500ºC, which is the maximum temperature of the dilatometer but is well below the samples' eutectic temperature (1578ºC). Nevertheless, it is evident that Ca-deficient samples densify better than Ca-rich, at least for the temperature range covered.

In order to explore further these two distinct behaviors, the two extreme CaO concentrations—i.e., as received (Ca/P=1.348) and 6 wt%-CaO-doped (Ca/P=1.52) powders—were selected to determine their optimal densification treatment. All samples were sintered at temperatures around their respective eutectic points for 2 and 6 hours. The results of this study are summarized in Figure 4. Ca-deficient samples could be steadily densified with substantial grain growth up to 1300ºC, slightly above their eutectic point—according to Figure 2, around 30 mol% liquid phase is expected to be present at this temperature—where a maximum density of around 92% of theoretical value was achieved. At higher temperatures, the increasing amount of liquid phase affects the shape-retention capacity of the samples and, therefore, such sintering treatments are not suitable for fabrication of our mold-free scaffolds. A similar effect is observed for Ca-rich samples at 1600ºC and above, despite the fact that barely a 10 mol% of liquid is expected for this

composition and temperature. At lower temperatures 90% of theoretical density could be achieved at most, with little associated grain growth.

Figure 5 shows the XRD results obtained for both powders (Fig. 5a) and sintered samples (Fig. 5b). It is evident that all starting powders, regardless of the pre-treatment performed on them, consist of β-TCP as the primary phase (Fig. 5a). A quick analysis of the results in Figure 5b reveals that in the Ca-rich sintered sample, the original β-TCP powder has transformed completely to α-TCP, which constitutes its primary phase. The presence of small amounts of calcium oxide phosphate (i.e. $Ca_4O(PO_4)_2$, denoted C_4P in Figure 2) can also be identified in the diffractogram. On the other hand, the pattern corresponding to the Ca-deficient sintered sample (Fig. 5b) shows that it consists of β-TCP as the primary crystalline phase, with a minor quantity of α-calcium pyrophosphate (i.e. α-$Ca_2P_2O_7$, denoted C_2P in Figure 2).

Figure 6 shows SEM micrographs corresponding to the microstructures of Ca-rich samples sintered at 1500ºC for 2 hours (Fig. 6a) and Ca-deficient samples sintered at 1300ºC for 2 hours (Fig. 6b), which are considered the optimal treatments (maximum density at the lowest temperature, time and grain growth without large macroscopic deformation) in each case. Differences in grain size are apparent just by comparing the scales in both micrographs. A secondary phase that results from the presence of liquid during sintering can be clearly observed in the Ca-deficient samples sintered at 1300°C (Fig. 6b). The liquid phase recrystallized, at least partially, during cooling or as a consequence of the thermal-etching treatment (1000ºC, 1 hour). Some microcracks can also be observed in Figure 6b. Similar microcracks have been reported by H.-S. Ryu et al. in Ca-deficient samples sintered above 1200ºC and are attributed to the expansion-contraction

cycle during a reversible β↔α transformation [18]. Theoretical densities for β-TCP and α-TCP are 3.07 and 2.86 g/cm^3, respectively.

These results demonstrate that the differences in the final densities and grain sizes for both types of specimens reflect the fact that densification of Ca-deficient samples is assisted by a liquid phase, while Ca-rich samples densify in solid state. Liquid phase sintering in Ca-rich samples could not be used to improve densification because the presence of a liquid phase in those samples immediately threatens their shape-retention capacity. The most probable explanation for this lack of tolerance to the presence of a liquid phase during sintering in Ca-rich samples is that, due to the higher temperatures at which the liquid appears, its viscosity is much lower than in the case of Ca-deficient samples (both liquids have a very similar composition). Such a low-viscosity liquid would quickly induce matter flow and shape changes in the sample. This is particularly critical for the robocasted grids, since deformation of the lines will significantly alter (and even close) the designed mesopore structure. Therefore, contrary to Ca-deficient samples, liquid-phase-assisted densification is not suitable for sintering robocasted Ca-rich TCP structures. In addition, it is evident from the XRD results that the sintering treatments used here for Ca-rich samples are not suitable for fabricating β-TCP scaffolds, because this phase transforms completely to α-TCP after sintering. In order to preserve the β phase, lower temperatures should be used—presumably below the transformation temperature of 1125ºC (Figure 2), and lower final densities are to be expected—a problem frequently reported in the literature [18-20]. By contrast, Ca-deficient samples maintain the β-TCP phase after sintering even at the highest temperature—well above 1125ºC. It has been recently suggested that the presence of $Ca_2P_2O_7$ simultaneously increases the β→α transition temperature and assists the inverse, α→β, transformation during cooling [18]. This could explain this phase

retention capacity of Ca-deficient samples. In any case, it is apparent that for Ca-deficient powders there is no need to limit the sintering treatment to temperatures below 1125ºC. Moreover, as we have shown, significant densifications can be easily achieved at 1300ºC by liquid phase sintering (LPS).

(2) Optimization of the ink

Colloidal inks developed for robocasting must satisfy two important criteria [12]: first, their viscoelastic properties must allow them to flow through a deposition nozzle and then "set" immediately so that shape is retained as additional layers are deposited, or when they span gaps in the underlying structure. Second, the suspensions must have a high solid volume concentration to minimize shrinkage during drying so that the particle network is able to resist the involved capillary stresses. The stability of these high-solids-loading suspensions requires high dispersive forces between particles [24,25], and therefore the role of dispersant is critical. The amount of dispersant has to be adjusted to efficiently coat the particles in the suspension, but an excess will cause flocculation of the particles due to the depletion effect [26]. On the other hand, as already mentioned, robocasting requires a pseudoplastic suspension with a yield stress high enough to prevent shape changes on the printed structure under its own weight. Therefore, the well-dispersed high-solids-loading suspensions are not yet functional for robocasting, even after the addition of the viscosifying agent (Methocel). Their rheology must be altered to form partially flocculated suspensions where a loosely bound particle network is formed [12]. In this study PEI was used as flocculant, to create the desired links between particles through interaction between its positively charged amine groups and the negatively charged carboxylic acid groups of the dispersant covering the TCP particles.

Consequently, the first step in the development of the inks was to determine the optimal amounts of dispersant and flocculant to be used. Following the procedure described in the experimental section, it was possible to determine that the optimal concentration of dispersant (corresponding to a minimum sediment height in the sedimentation tests) is around 1.5% relative to powder weight. The optimal amount of PEI was estimated to be around 0.4 wt% relative to water content (maximum sediment height). The final tuning of the viscoelastic properties of the suspension is achieved by slightly adjusting its pH with HNO_3 or NH_4OH as needed. The pH of the suspension controls the activity of both dispersant and flocculant and, therefore, the strength of the bonds between the particles and its ability to form the desired network. For hydroxyapatite the optimum pH has been shown to be ~9 [27].

Once the optimal concentration of organics in the suspension is known, it is necessary to determine the maximum solid content practical for robocasting inks. It was found that 45 wt% is the optimal solid content, and that very little range of variation was possible around this value. Inks prepared with higher solid-loading exhibited very limited printability and lower concentrations led to poor shape-retention capacity.

After optimizing the composition of the ink, the only variable affecting the ink performance that remained unexplored was the morphology and grain size of the powder. It was initially observed that the inks prepared from the as-received commercial powders exhibited very poor overall performance compared to those formulated with the CaO-doped powders fabricated for the sintering study. These differences could not be attributed to the slight change in composition of the powder but, more likely, to a change in its morphology as a consequence of the heat treatment employed to promote the TCP-$CaCO_3$ reaction. To

verify this hypothesis, certain amounts of as-received powder were calcined at 1000ºC for 2 and 6 hours. All inks prepared from calcined powders showed improved behavior, although those fabricated from powders calcined for 6 hours performed slightly better. No loss of mass or change in the XRD pattern of the powder was observed after calcination (Fig. 6a), but the powder morphology changed significantly. Figures 7a and 7b show SEM micrographs of the β-TCP powders before and after calcination for 6 hours, respectively. It is apparent that the morphology of the powder changes with calcination from sharply faceted grains to round particles. This reduction in the specific surface area could explain the improved performance of the inks fabricated from calcined powders, as it will facilitate both the adsorption of the dispersant—which both increases suspension stability and the effectiveness of PEI to form the loosely bonded particle net—and the close packing of the particles within the ink. Effects of calcination on the performance of inks for robocasting has recently been reported for the case of HA [27], though in that case improvements upon calcination have been attributed to a densification of the porous HA agglomerates that hampered the formulation of inks with high solid content.

Unfortunately, the change in morphology of β-TCP powders during calcination is accompanied by a twofold increase in the average particle size, from the starting 1.8 ± 0.8 μm to 4 ± 1 μm as measured by centrifugal photo-sedimentation, mainly due to the formation of hard aggregates. Larger particles mean reduced suspension stability (i.e., shorter precipitation time) and, thereby, lower printability of the final ink. To avoid this problem, the calcined powder was placed in an attritor mill for 1 hour at 450 rpm to reduce particle size back to 2.2 ± 0.8 μm. Figure 7c shows the morphology of the resulting powder. With this additional powder refinement step, the resulting inks performed satisfactorily.

The role of the starting powder on the ink performance is critical. In fact, although optimizing the rest of the intervening parameters (organics composition, solid content, pH, etc) is certainly necessary, using a powder with inadequate size or morphology will hamper all attempts to fabricate a suitable ink. Indeed, it is evident from our results that reduced size and round and smooth surfaces are preferred features of the starting powders in the preparation of inks for robocasting.

(3) Fabrication and characterization of the scaffolds

The results from the sintering study indicate that, in order to obtain a scaffold with dense β-TCP lines fabricated by robocasting, calcined and milled Ca-deficient powders should be used, and that the optimal sintering treatment at 1300ºC for 2 hours yields a maximum density of about 92 % th. Therefore, in this work β-TCP scaffolds were fabricated by robocasting following this sintering route. Several printing speeds were used to elucidate their effect on the quality of the final scaffolds, and it was found that acceptable structures—i.e., with the minimum number of printing defects—could be printed up to a maximum in-plane printing speed of 30 mm/s, though the most sensible speeds were 10-20 mm/s. These values would depend on factors like the number of residual bubbles or the viscoelastic properties of the ink and therefore should only be taken as a rough guideline. The morphology after sintering of one of the samples printed at 10 mm/s speed through a tip of 250 μm diameter is shown in Figure 8. An average linear shrinkage of around 20% was measured after sintering, and the final line diameter is about 200 μm, while the spacing between lines is around 75 μm. Typically, robocasting is a suitable technique for fabricating spanning structures with characteristic feature sizes (i.e., line diameter and spacing) ranging from ~100 μm to ~1 mm [12], although it may be possible to assemble 3-D periodic structures with finer or broader features if the proper ink can be

produced. The microstructure shown in Figure 8e coincides with that of the bulk samples (cf. Fig. 6b). The presence of micro-cracks is evident in both micrographs, and grain size measurements yielded similar results in both cases.

Despite these microstructural similarities, the results from microindentation tests show that the mechanical properties of the scaffolds do not match those of the bulk samples. Instead, contrary to what one might expect a priori, the printed rods show an almost twofold increase in hardness over bulk isostatically pressed β-TCP samples: 3.7 ± 0.6 GPa compared to 2.0 ± 0.6 GPa. This increase in hardness cannot be explained in terms of microstructural changes or density variations, as is evident in comparing Figures 6b and 8e. Consequently, its origin is attributed to the existence of compressive residual stresses in the printed samples, generated during the drying and sintering process. Toughness could not be estimated from the indentation tests, because no well-developed cracks appeared at the corners of the imprints. Instead, especially in the printed samples, numerous smaller cracks—generated probably from pre-existing microcracks, such as those that can be clearly observed in Figures 6b and 8e—appeared surrounding the whole imprint. This could indicate a certain degree of resistance against the propagation of well-developed cracks, although further measurements need to be carried out to verify this extreme. Nevertheless, the fact that the hardness of printed β-TCP rods is larger than that of equivalent bulk materials supports the conclusion that robocasting is a promising technique for the fabrication of ceramic scaffolds.

Our preliminary tests indicate that the compressive strength of the robocasted grids is 10 to 20 MPa in all testing directions (parallel and perpendicular to the printing plane). This is of the order of porous calcium phosphates with similar porosity (~ 45 %) fabricated

by conventional techniques [28] and close to the corresponding value for cancellous bone (7-10 MPa) [29]. No de-bonding of the lines was observed during testing, indicating excellent adhesion between them. Further mechanical characterization is under way in order to better assess the relationship between processing conditions, mesostructural design and mechanical response.

IV. CONCLUSIONS AND IMPLICATIONS

β-TCP scaffolds consisting of a 3-D network of rods with tailored geometry and mesoscale porosity have been fabricated by direct-write assembly. To achieve this goal, concentrated β-TCP inks suitable for this fabrication route have been obtained and optimized. Powder size and morphology have been shown to play a major role in ink performance, so that powders with reduced particle size and low specific surface area are more suitable for ink preparation.

The sintering behavior of β-TCP was also studied as a function of the calcium content present in the starting powder, and the optimal heat treatment for obtaining dense β-TCP scaffolds by mold-free techniques such as robocasting was determined. It has been shown that, in order to prevent the β→α transition of the TCP during densification, Ca-deficient powders should be used for ink preparation. It is worth noting that by controlling the composition of the starting powders and the sintering temperature it is possible to manipulate the composition of the scaffold (i.e, the relative amount of α and β–TCP and presence of amorphous phases), and the microporosity of the printed lines. This opens a way to systematically manipulate the degradation rates and prepare materials with an

optimum combination of mechanical properties and biorresorption. Control of the microporosity and roughness of the lines will also help to manipulate cell attachment and osseointegration, issues that will be addressed in future work. Further control of the scaffold properties can be achieved by printing composite structures using several injector heads with inks of different Ca content or with different phases. Whatever the case may be, the results obtained in this future work would be valuable in tailoring the performance of TCP scaffolds fabricated by direct-write assembly for bone tissue engineering.

ACKNOWLEDGEMENTS

This work was supported by the National Institutes of Health (NIH) under Grant No. 5R01 DE015633. Pedro Miranda wants to acknowledge financial support from the European Community's Sixth Framework Program under a Marie Curie Outgoing International Fellowship (MOIF-CT-2005-7325).

REFERENCES

1. Langer R, Vacanti JP. Tissue engineering. Science 1993;260:920-6.
2. Hutmacher DW. Scaffolds in tissue engineering bone and cartilage. Biomaterials 2000;21:2529-2543.
3 Sachlos E, Czernuszka JT. Making tissue engineering scaffolds work. Review on the application of solid freeform fabrication technology to the production of tissue engineering scaffolds. European Cells and Materials 2003;5:29-40.
4 Pham DT, Dimov SS. Rapid prototyping processes. In: Pham DT, Dimov SS., editors. Rapid Manufacturing: the Technologies and Applications of Rapid Prototyping and Rapid Tooling. London: Springer; 2000. p 19-42.

5 Rekow DE, Erdman AG, Riley D, Klamecki B. CAD/CAM for dental restorations—some of the curious challenges. IEEE Trans Biomed Eng 1991;38(4):314–8.

6 Hutmacher DW. Scaffolds in tissue engineering bone and cartilage. Biomaterials 2000;21:2529–43.

7 Langton CM, Whitehead MA, Langton DK. Development of a cancellous bone structural model by stereolithography for ultrasound characterization of the calcaneus. Med Eng Phys 1997;19:599.

8 Chu T-MG, Orton DG, Hollister SJ, Feinberg SE, Halloran JW. Mechanical and in vivo performance of hydroxyapatite implants with controlled architectures. Biomaterials 2002;23:1283–93.

9 Hollister S. Porous scaffold design for tissue engineering. Nat Mat 2005;4:518-524.

10 Cesarano III J, Calvert P. Freeforming Objects with Low-Binder Slurry. US Patent 6,027,326.

11 Cesarano III J, Segalman R, Calvert P. Robocasting provides moldless fabrication from slurry deposition. Ceram Ind 1998;148(4):94-102.

12 Smay JE, Cesarano III J, Lewis JA. Colloidal inks for directed assembly of 3-D periodic structures. Langmuir 2002;18:5429-5437.

13 Hench LL. Bioceramics: from concept to clinic. J Am Ceram Soc 1991;74(7):1487–510.

14 Hench LL. Bioceramics. J Am Ceram Soc 1998;81(7):1705–28.

15 Nancollas GH. Formation and dissolution mechanisms of calcium phosphates in aqueous systems. In: Brown PW, Constantz B, editors. Hydroxyapatite and Related Materials. Boca Raton: CRC Press, Inc.; 1994. p 74.

16. Lacefield WR. Hydroxylapatite Coatings. In: Hench LL, editor. An Introduction to Bioceramics. Singapore: World Scientific; 1993. p 223-238.

17. Klein CPAT, Wolke JGC, de Groot K. Stability of calcium phosphate ceramics and plasma spray coating. In: Hench LL, Wilson J, editors. An Introduction to Bioceramics. Singapore: World Scientific; 1998. p 199-221.

18 Ryu H-S, Youn H-J, Hong KS, Chang B-S, Lee C-K, Chung S-S. An improvement in sintering property of β-tricalcium phosphate by addition of calcium pyrophosphate. Biomaterials 2002;23:909–914.

19 Itatani K, Nishioka T, Seike S, Howell FS, Kishioka A, Kinishita M. Sinterability of β-calcium orthophosphate powder prepared by spray-pyrolysis. J Am Ceram Soc 1994;77(3):801–5.

20 Famery R, Richard N, Boch P. Preparation of α- and β- tricalcium phosphate ceramics, with and without magnesium addition. Ceram Int 1994;20:327–36.

21 Akao M, Aoki K, Kato K, Sato A. Dense polycrystalline β-tricalcium phosphate for prosthetic applications. J Mater Sci 1982;17:343-346.

22 Reed JS. Principles of Ceramic Processing. New York: Wiley; 1995.

23 Kreidel ER, Hummel FA. Inorg Chem 1967;6(5):891. In: Phase Diagrams for Ceramists, Vol. II, edited by the American Ceramic Society; 1969. p 85.

24 Cesarano III J, Aksay IA. Processing of highly concentrated aqueous α-alumina suspensions stabilized with polyelectrolytes. J Am Ceram Soc 1988;71(12):1062–1067.

25 Lange FF. Colloidal processing of powder for reliable ceramics. Curr Opin Solid State Mater Sci 1998;3(5):496–500.

26 Stuecker JN, Cesarano III J, Hirschfeld DA. Control of the viscous behavior of highly concentrated mullite suspensions for robocasting. J Mater Process Tech 2003;142:318–325.

27 Michna S, Wu W, Lewis JA. Concentrated hydroxyapatite inks for direct-write assembly of 3-D periodic scaffolds. Biomaterials 2005;26(28):5632-5639.

28 Deville S, Saiz E, Nalla RK, Tomsia AP. Freezing as a path to build complex composites. Science 2006;311(5760):515-518.

29 Murugan R, Ramakrishna S. Development of Nanocomposites for bone grafting. Composites Science and Technology 2005; 65 (15-16):2385-2406.

FIGURE CAPTIONS

1. Schematic of robocasting fabrication process. The ceramic part is built layer-by-layer from a computer design. A 3-axis robotic arm moves the injection syringe while pressing the ceramic ink through the conical deposition nozzles, immersed in an oil bath to create a self-supporting 3-D network.

2. Partial CaO-P_2O_5 equilibrium phase diagram [23]. For the sake of clarity the following notation is adopted to identify phase composition: C=CaO, P=P_2O_5. Dashed lines indicate the two extremes of the range of compositions analyzed in this work.

3. Sintering strain of β-TCP green compacts prepared by cold isostatic pressing (heating rate 3ºC/min) during dynamic dilatometry. Solid and dashed lines represent Ca-deficient (Ca/P < 1.5) and Ca-rich (Ca/P > 1.5) samples, respectively.

4. Final densities and grain sizes of sintered samples fabricated from as-received (Ca/P=1.348) and 6 wt%-CaO-doped (Ca/P=1.52). Relative density and porosity are represented as a column bar graph (left Y-axis) and the grain sizes (mean linear intercept lengths) are included as solid circles (right Y-axis), with error bars representing standard deviation of the data. Theoretical densities of 3.07 and 2.86 g/cm^3 are considered for β-TCP (Ca-deficient) and α-TCP (Ca-rich), respectively.

5. XRD patterns corresponding to a) starting powders and b) sintered samples of Ca-rich (Ca/P=1.52) and Ca-deficient (Ca/P=1.348) materials after optimal densification treatment (2 hours at 1500ºC and 1300ºC, respectively). All starting powders are identified as β-TCP. After sintering, α-TCP is the primary phase present in the Ca-rich sintered samples, with a small amount of a secondary oxide calcium phosphate (i.e. $Ca_4O(PO_4)_2$, denoted C4P). Ca-deficient sintered samples consist of β-TCP with a minor quantity of α-calcium pyrophosphate (i.e. α-$Ca_2P_2O_7$, denoted C2P).

6. SEM micrographs (after thermal etching for 1 hour at 1000ºC) showing the microstructures of sintered samples with maximum density: a) Ca-rich (Ca/P=1.52) sintered at 1500ºC for 2 hours and b) Ca-deficient (Ca/P=1.348) sintered at 1300ºC for 2 hours. Differences in grain size are apparent (note scales). Note also the clearer secondary phase in b), revealing the presence of liquid during sintering of Ca-deficient samples. Arrows in b) mark the presence of microcracks.

7 SEM micrographs of the β-TCP commercial powders: (a) as-received, (b) after calcination at 1000ºC for 6 hours and (c) attritor-milled for 1 hour at 450 rpm after calcination at 1000ºC for 6 hours. Note the significant change in the powder morphology after calcination: the grains become rounder and smoother and the specific surface area decreases.

8. Representative SEM micrographs showing β-TCP (Ca/P=1.348) scaffold morphology after sintering at 1300ºC for 2 hours: a) general view, b) XY plane view, c) detail of the β-TCP rods, d) detail of the rod surface and e) cross-section

view showing the microstructure within the rods. Note in e) the presence of microcracks (marked by arrows) and the clearer secondary phase related to liquid present during sintering (cf. Fig. 6b).

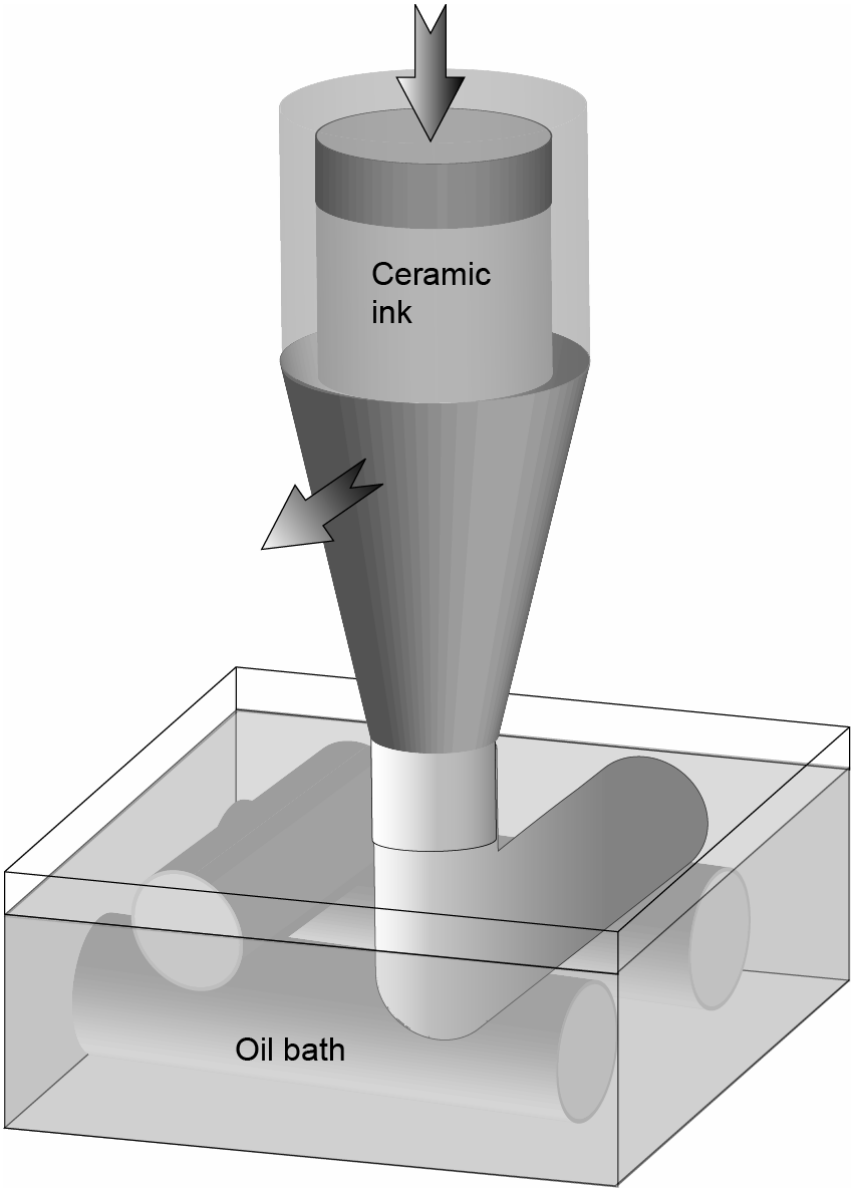

Fig. 1

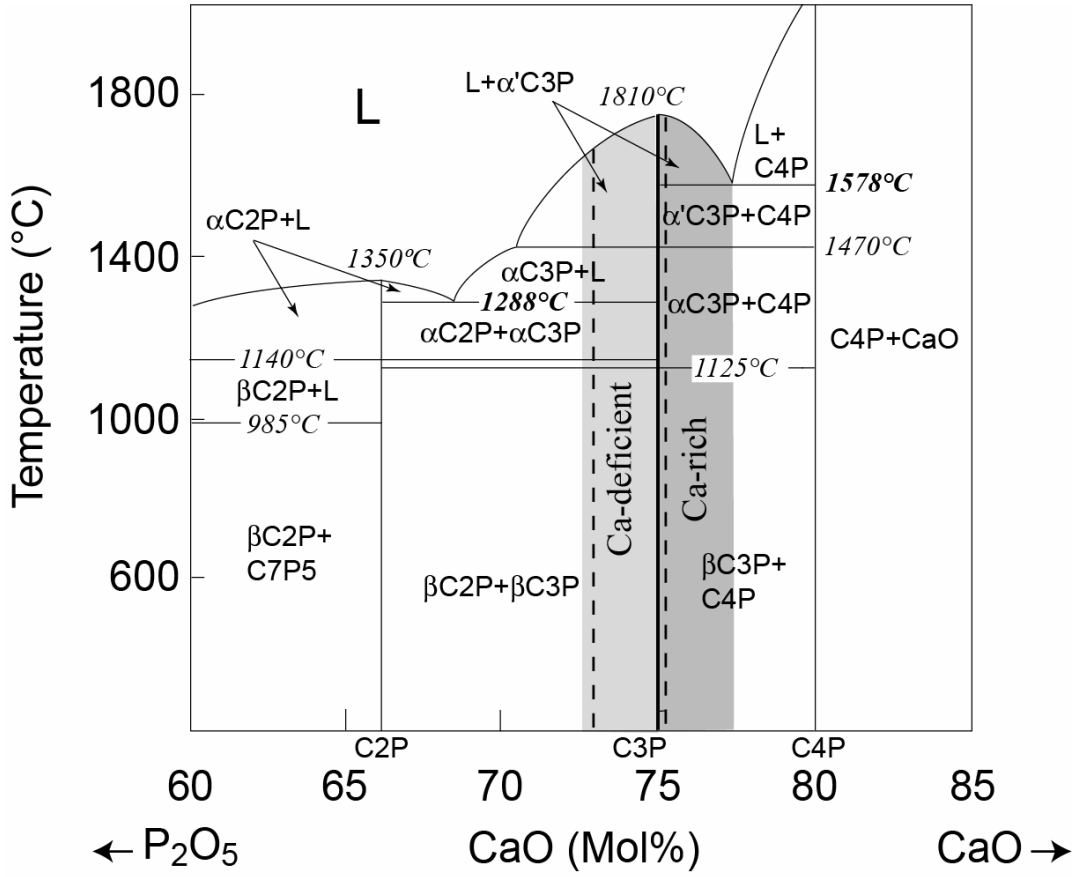
Temperature (°C)
1800
1400
1000
600
L
L+α'C3P
1810°C
L+
C4P
1578°C
α'C3P+C4P
1470°C
αC2P+L
1350°C
αC3P+L
1288°C
αC3P+C4P
αC2P+αC3P
C4P+CaO
1140°C
1125°C
βC2P+L
985°C
Ca-deficient
Ca-rich
βC2P+
C7P5
βC2P+βC3P
βC3P+
C4P
C2P
C3P
C4P
60
65
70
75
80
85
← P2O5
CaO (Mol%)
CaO →

Fig. 2

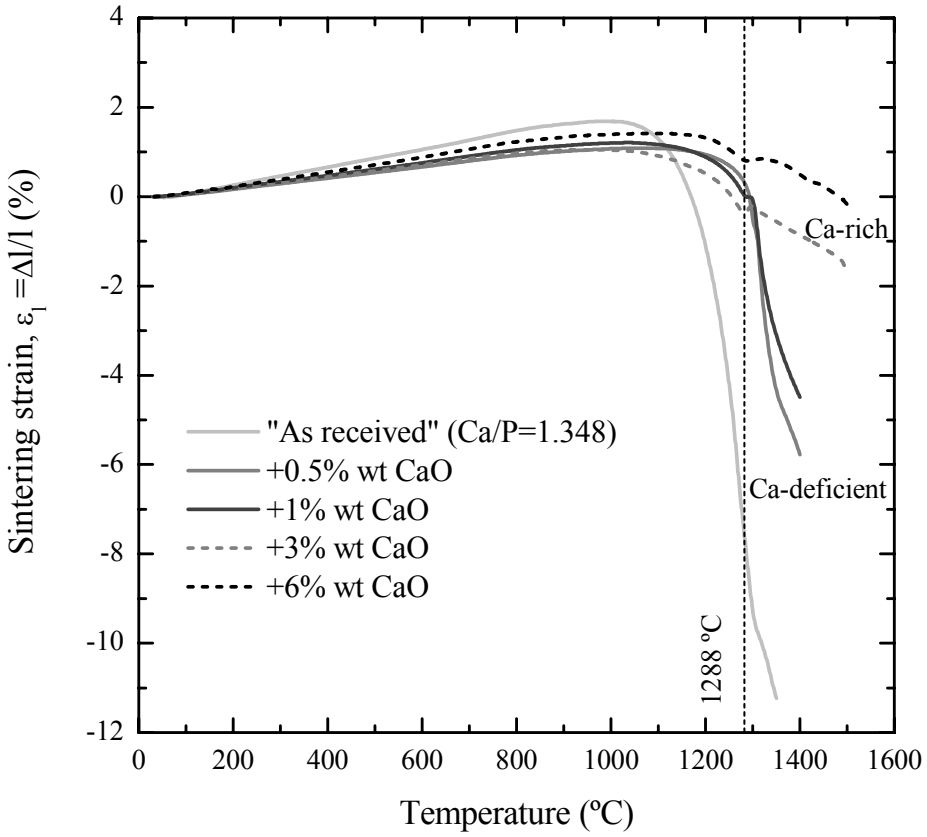
Sintering strain, $\varepsilon_l = \Delta l/l$ (%)
Temperature (ºC)
"As received" (Ca/P=1.348)
+0.5% wt CaO
+1% wt CaO
+3% wt CaO
+6% wt CaO
Ca-rich
Ca-deficient
1288 ºC
4
2
0
-2
-4
-6
-8
-10
-12
0
200
400
600
800
1000
1200
1400
1600

Fig. 3

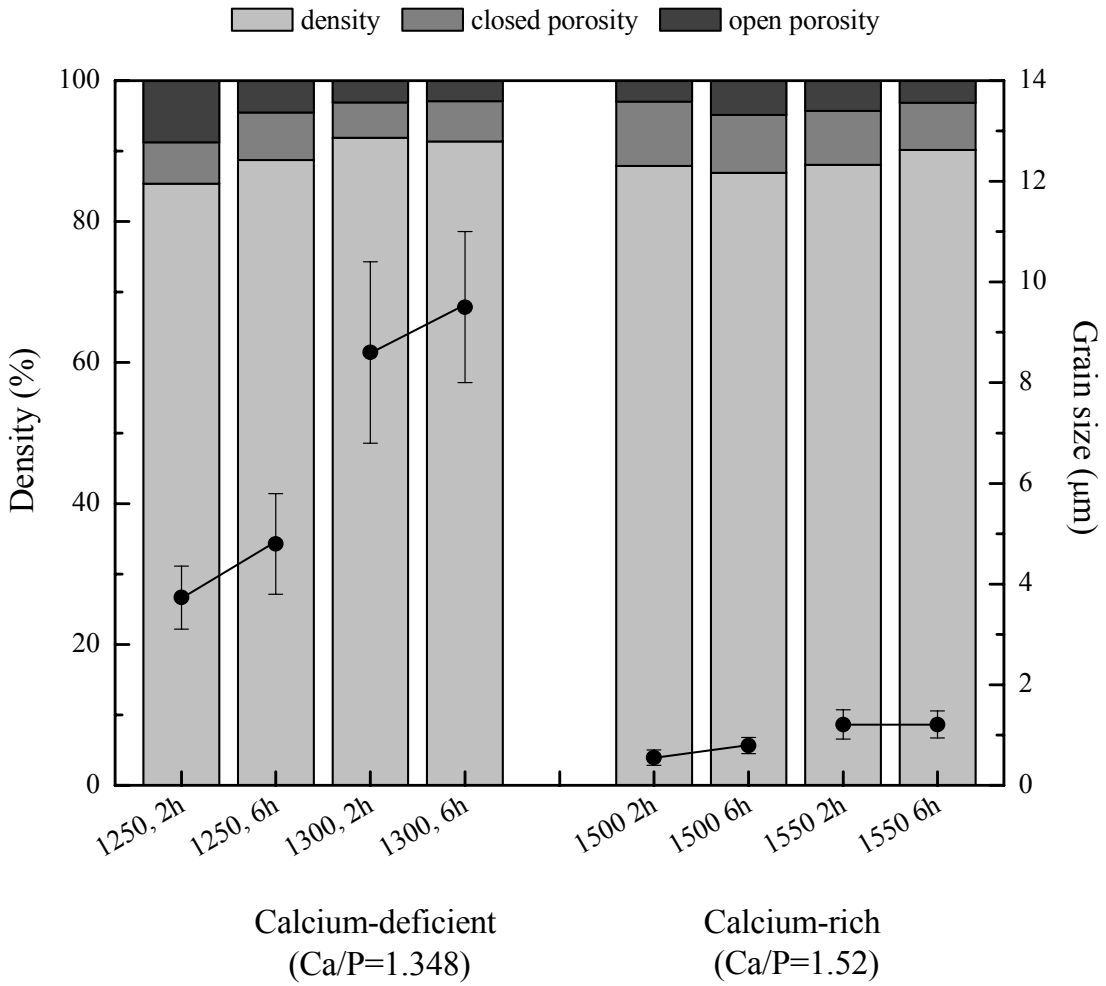
density
closed porosity
open porosity
Density (%)
Grain size (μm)
0
20
40
60
80
100
0
2
4
6
8
10
12
14
1250, 2h
1250, 6h
1300, 2h
1300, 6h
1500 2h
1500 6h
1550 2h
1550 6h
Calcium-deficient
(Ca/P=1.348)
Calcium-rich
(Ca/P=1.52)

Fig. 4

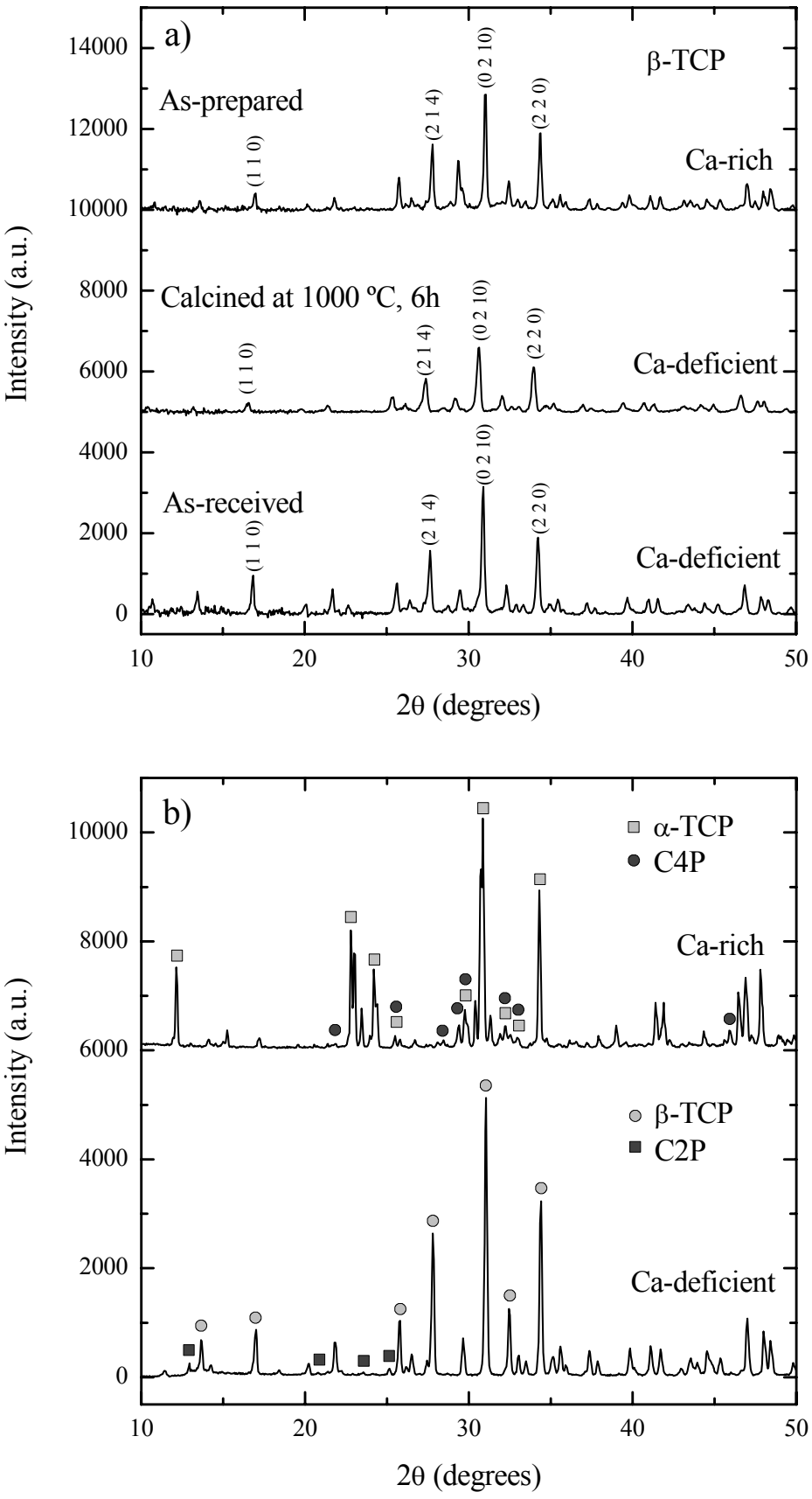
a)
β-TCP
As-prepared
Ca-rich
Calcined at 1000 ºC, 6h
Ca-deficient
As-received
Ca-deficient
(1 1 0)
(2 1 4)
(0 2 10)
(2 2 0)
Intensity (a.u.)
2θ (degrees)
b)
α-TCP
C4P
Ca-rich
β-TCP
C2P
Ca-deficient
Intensity (a.u.)
2θ (degrees)

Fig. 5

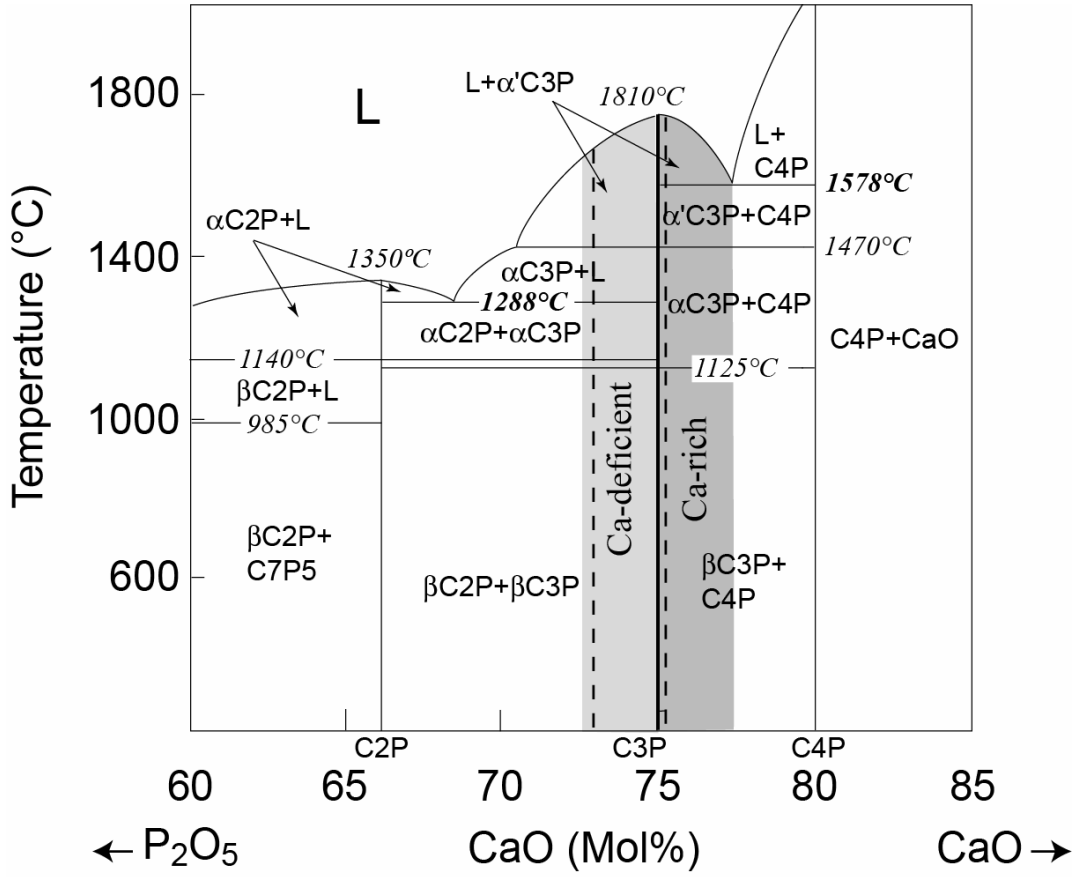
Temperature (°C)
1800
1400
1000
600
L
L+α'C3P
1810°C
L+
C4P
1578°C
α'C3P+C4P
1470°C
αC2P+L
1350°C
αC3P+L
1288°C
αC3P+C4P
αC2P+αC3P
C4P+CaO
1140°C
1125°C
βC2P+L
985°C
Ca-deficient
Ca-rich
βC2P+
C7P5
βC2P+βC3P
βC3P+
C4P
C2P
C3P
C4P
60
65
70
75
80
85
← P2O5
CaO (Mol%)
CaO →

Fig. 2

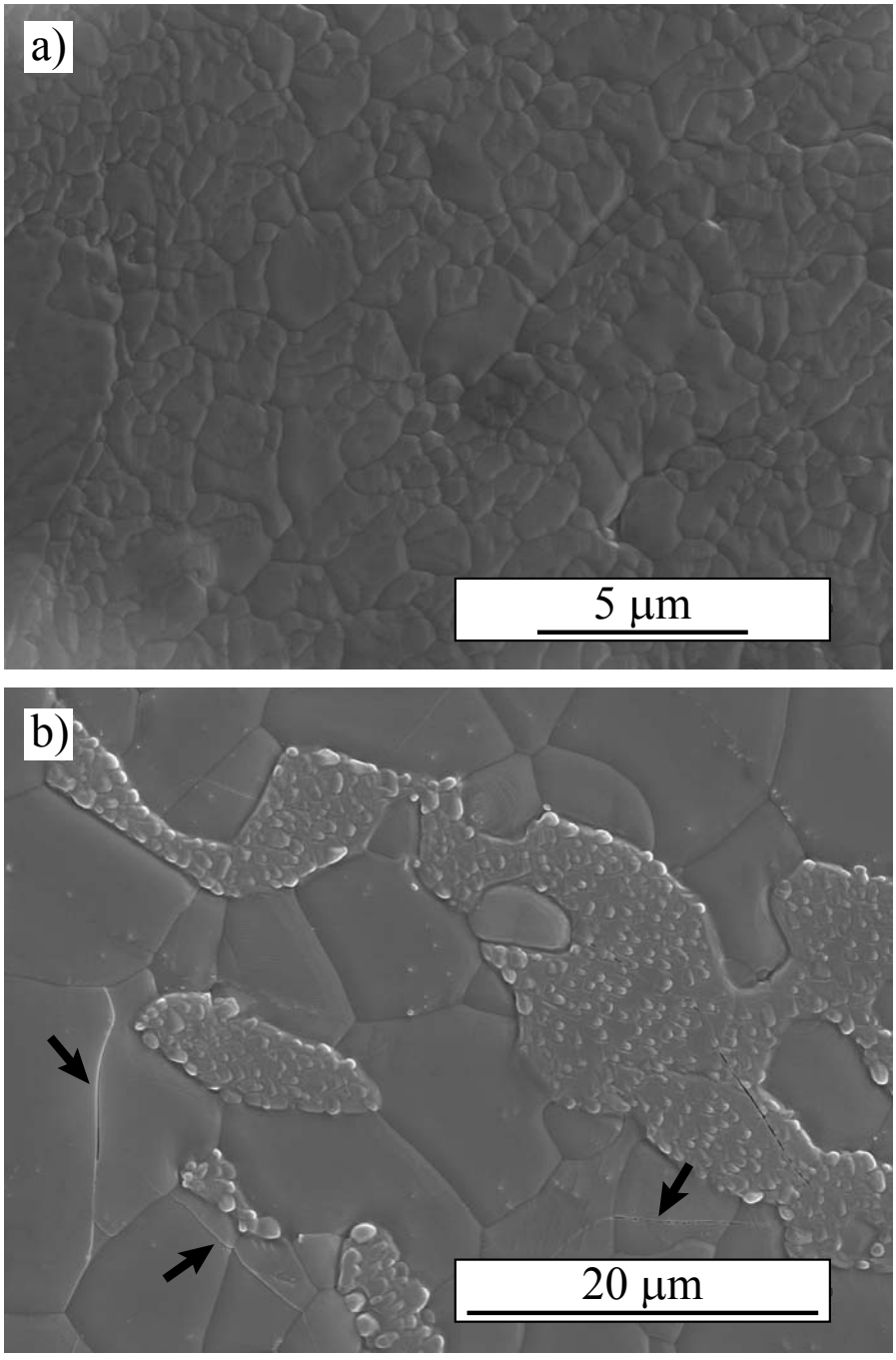

Fig. 6

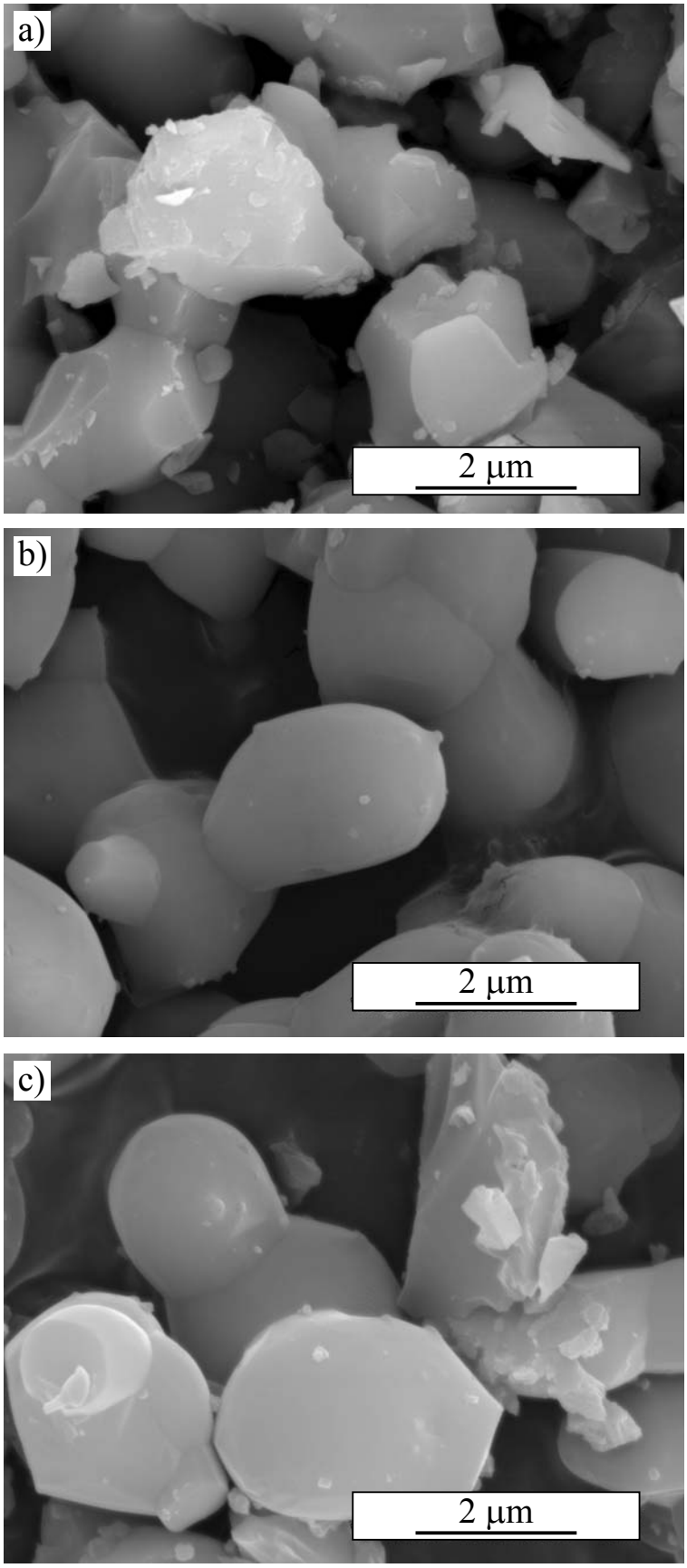

Fig. 7

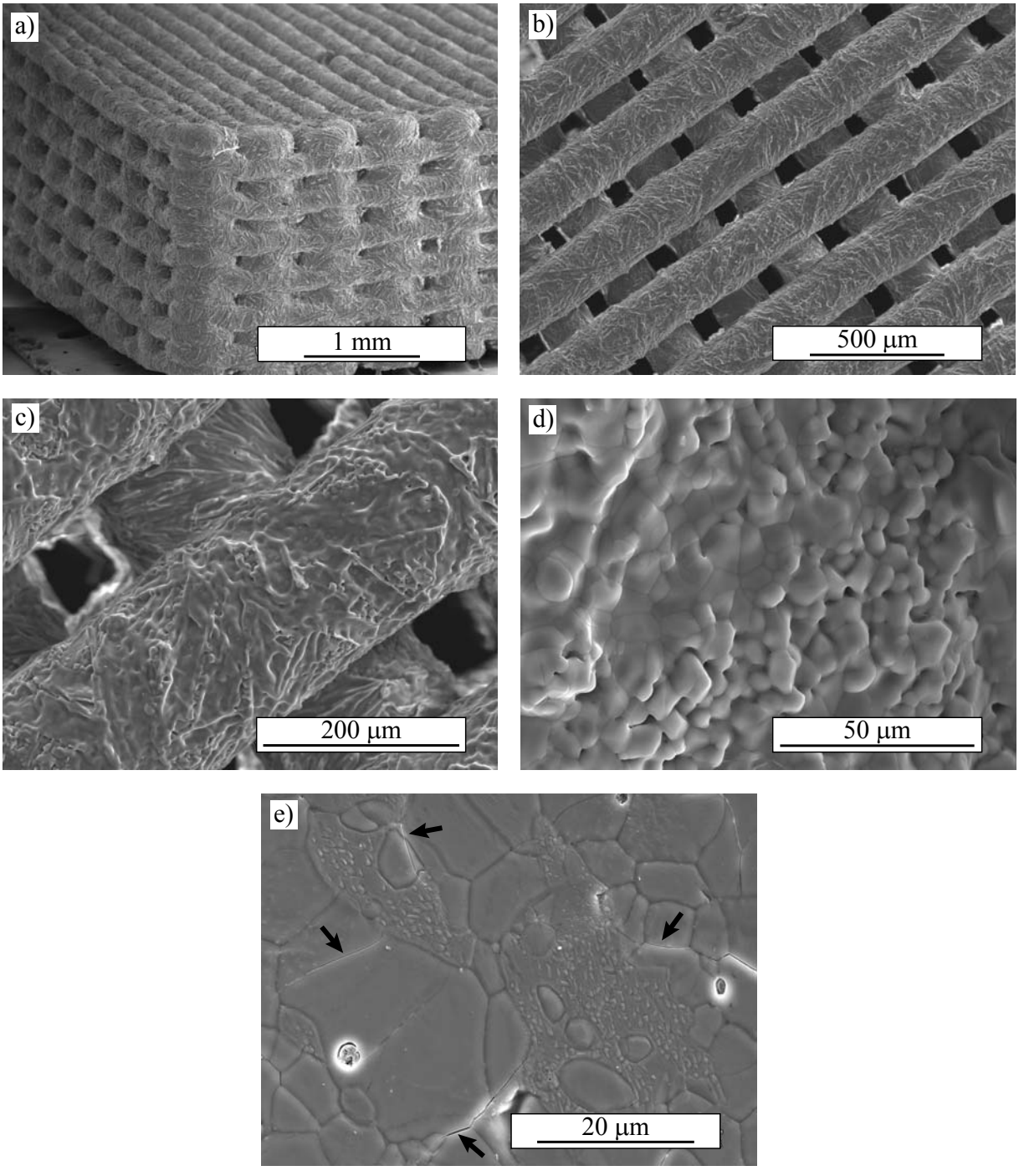

Fig. 8

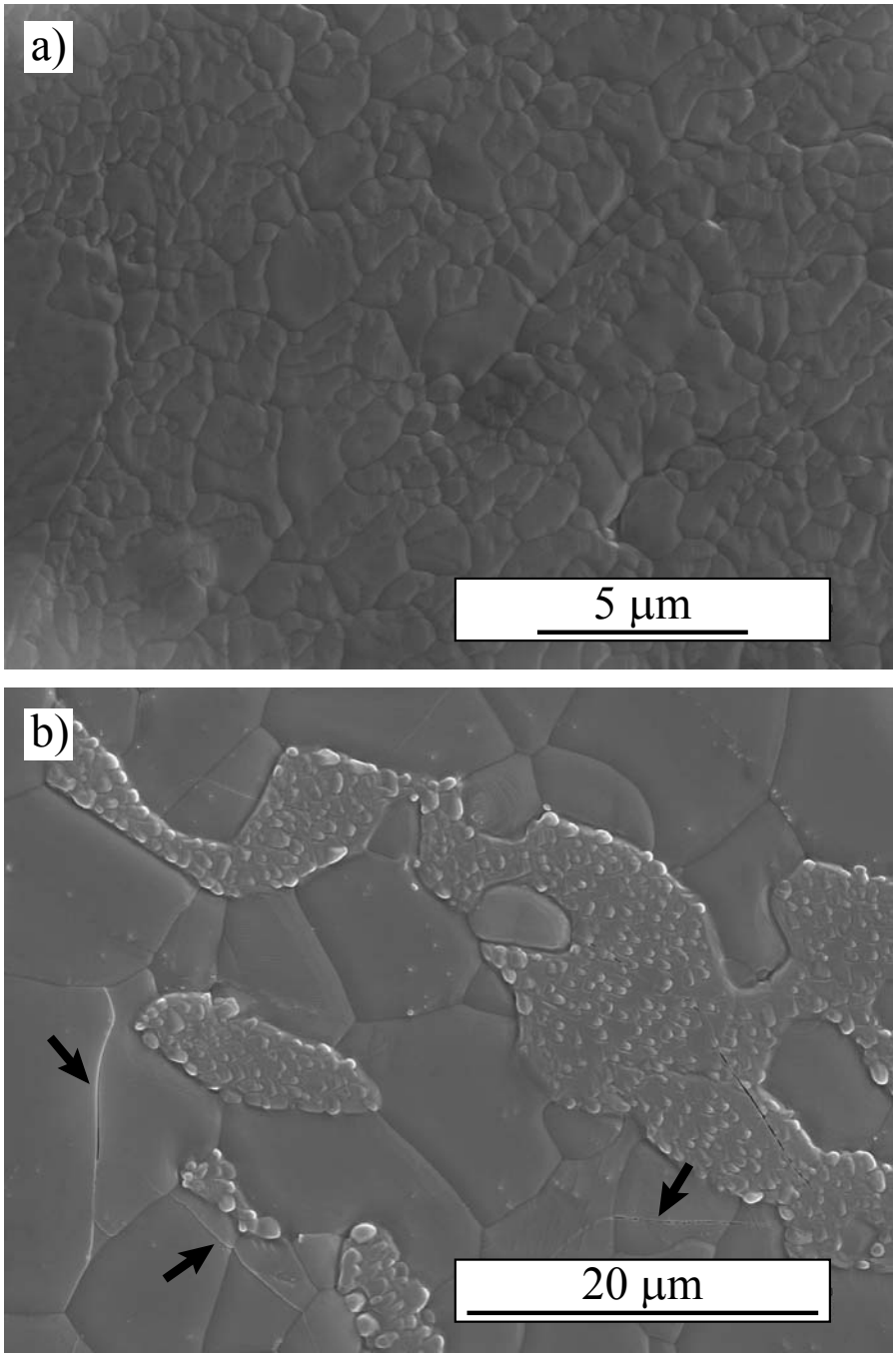

Fig. 6

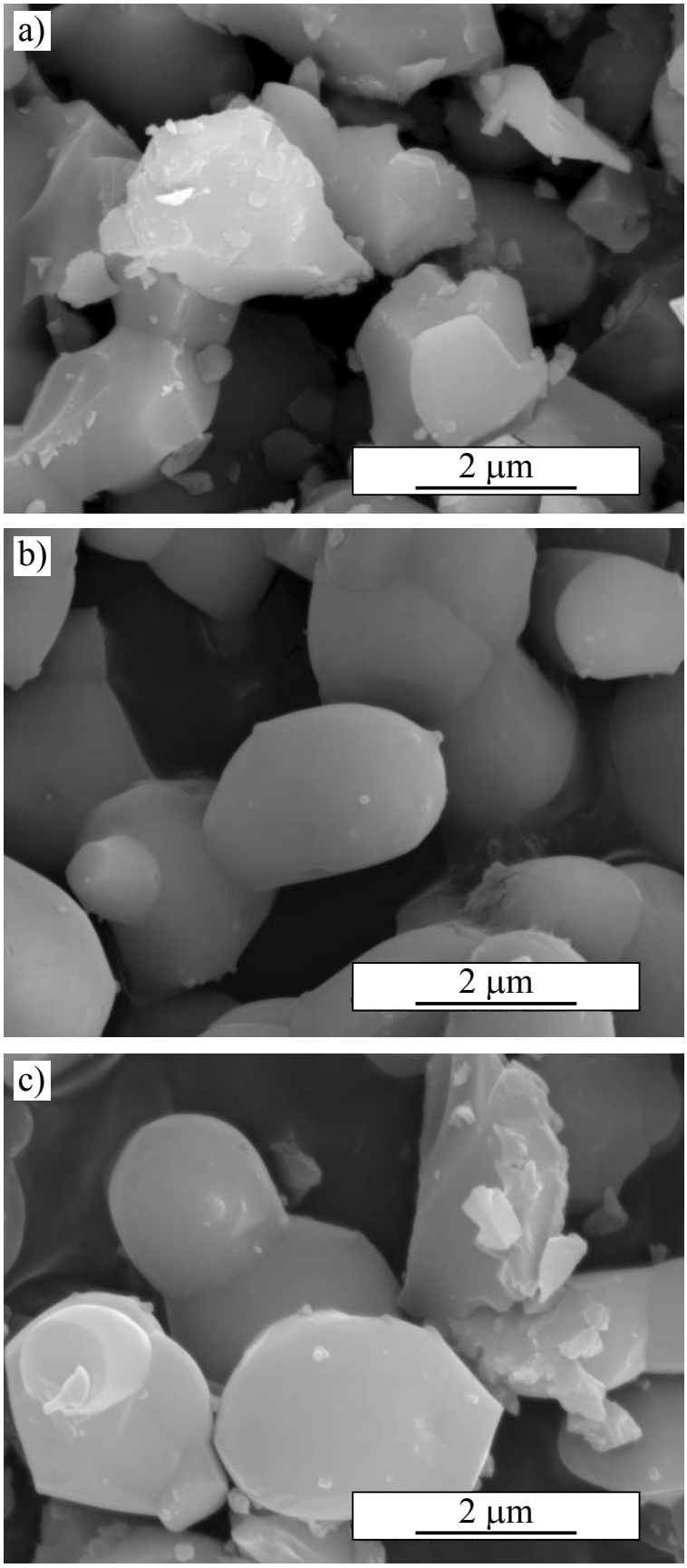

Fig. 7

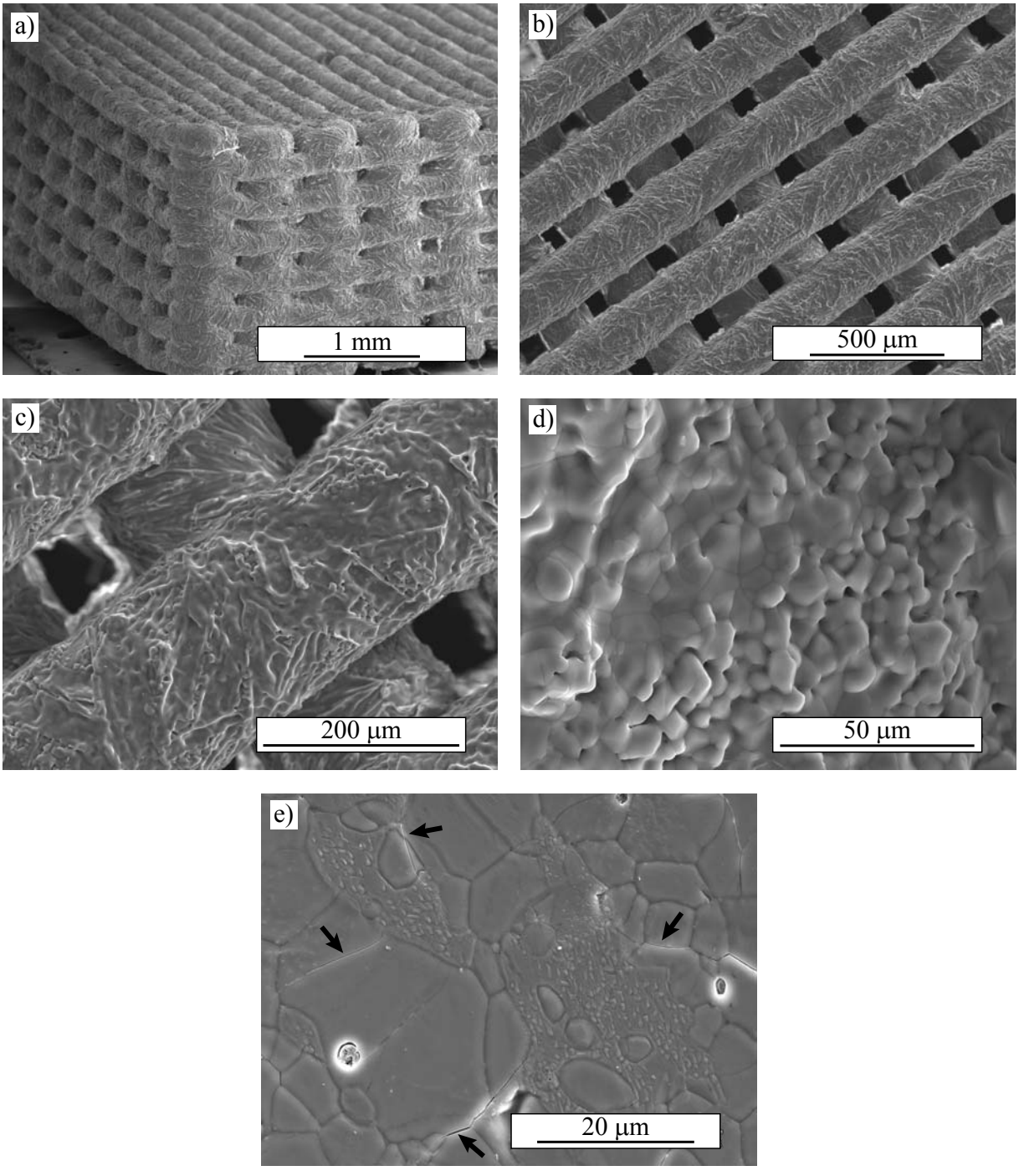

Fig. 8